Electronic Supplementary Material (ESI) for CrystEngComm.
This journal is © The Royal Society of Chemistry 2024

Supporting Information

Dual modifications of sensitizers and lanthanide ions on a two-dimensional zirconium-based metal–organic framework for photoluminescent detection

Jhe-Wei Chang,[a] Tzu-Chi Lin,[a] You-Liang Chen,[a] Po-Chun Han,[b] Shang-Cheng Yang,[a] Meng-Dian Tsai,[a] Kevin C.-W. Wu [b,c,d] and Chung-Wei Kung *[a]

[a] Department of Chemical Engineering, National Cheng Kung University, Tainan City, Taiwan, 70101.

[b] Department of Chemical Engineering, National Taiwan University, Taipei, Taiwan, 10617.

[c] Ph. D. Program of Green Materials and Precision Devices, College of Engineering, National Taiwan University, Taipei 10617, Taiwan.

[d] Department of Chemical Engineering and Materials Science, Yuan Ze University, Chung-Li, Taoyuan 320, Taiwan.

*Email: cwkung@mail.ncku.edu.tw

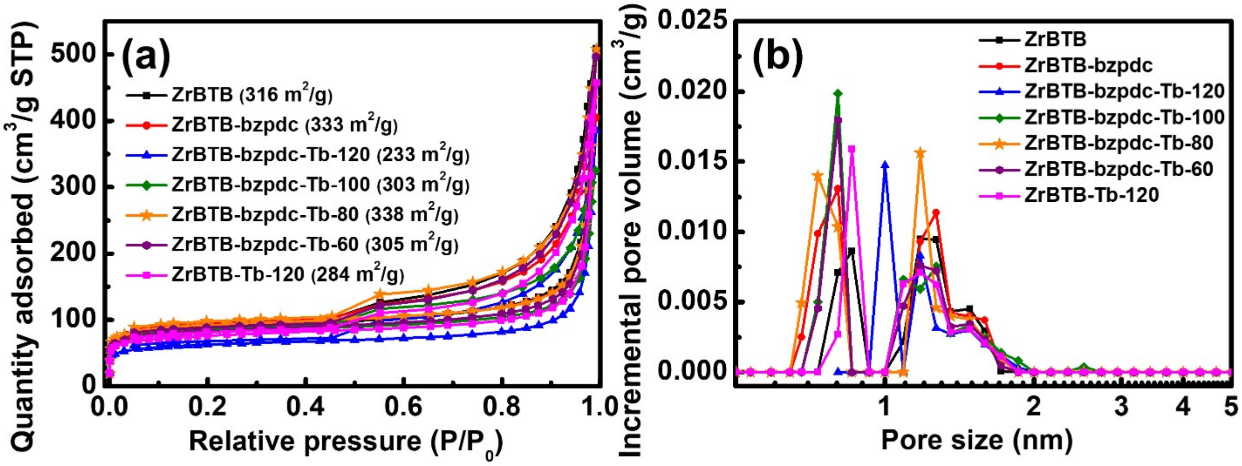

Figure S1. (a) Nitrogen adsorption-desorption isotherms measured at 77 K and (b) corresponding DFT pore size distributions of all 2D MOF-based materials. Calculated BET surface areas are listed in (a). Pore size distributions were extracted from isotherms shown in (a) by using the model of carbon slit pore.

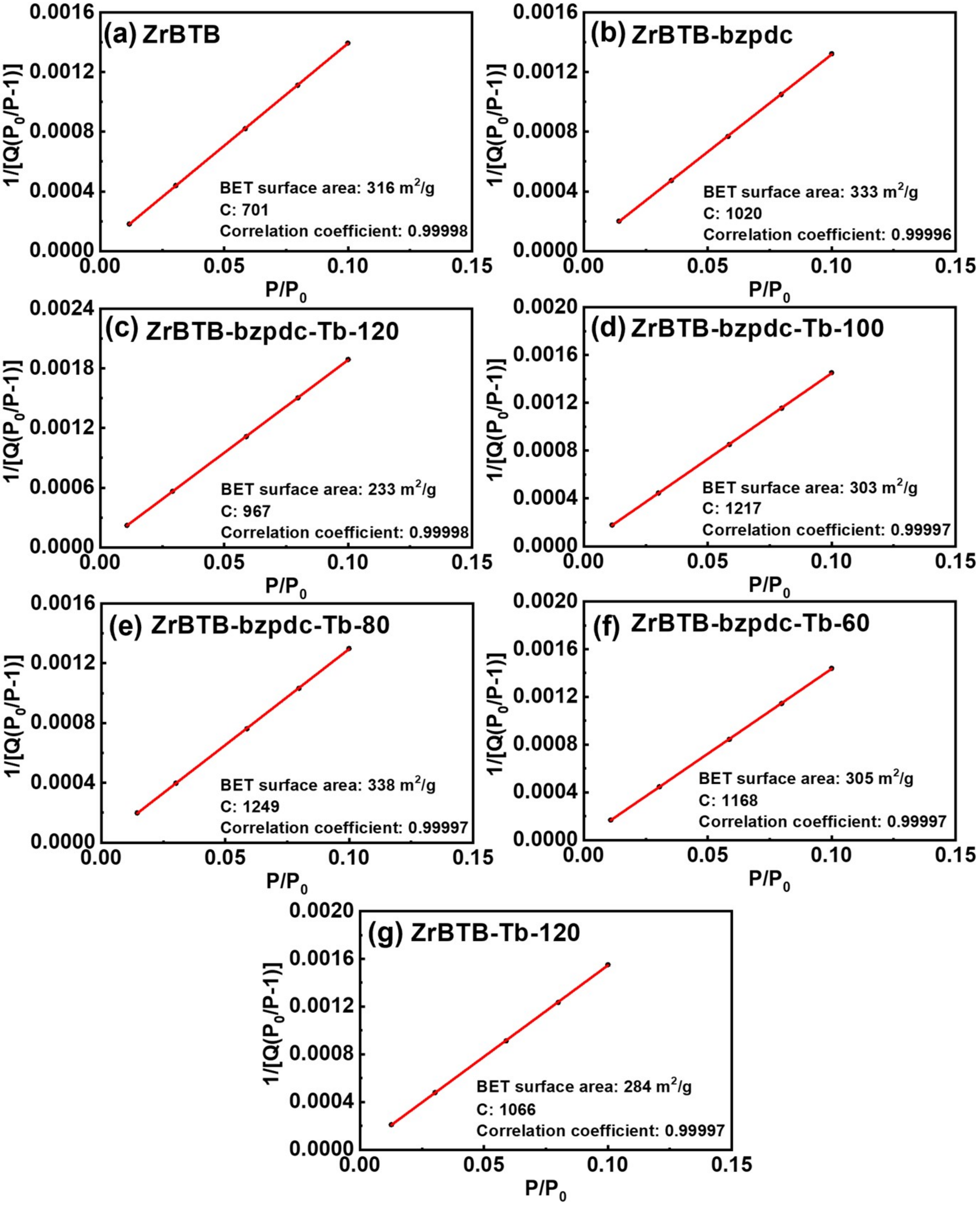

Figure S2. Plots for calculating BET surface areas of (a) ZrBTB, (b) ZrBTB-bzpdc, (c) ZrBTB-bzpdc-Tb-120, (d) ZrBTB-bzpdc-Tb-100, (e) ZrBTB-bzpdc-Tb-80, (f) ZrBTB-bzpdc-Tb-60 and (g) ZrBTB-Tb-120, with C values and correlation coefficients.

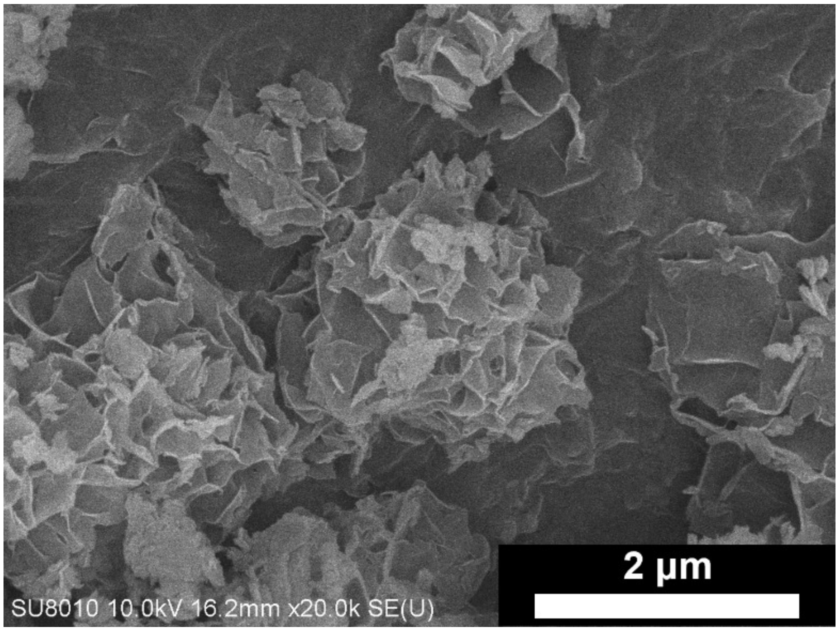

Figure S3. Representative SEM image of ZrBTB.

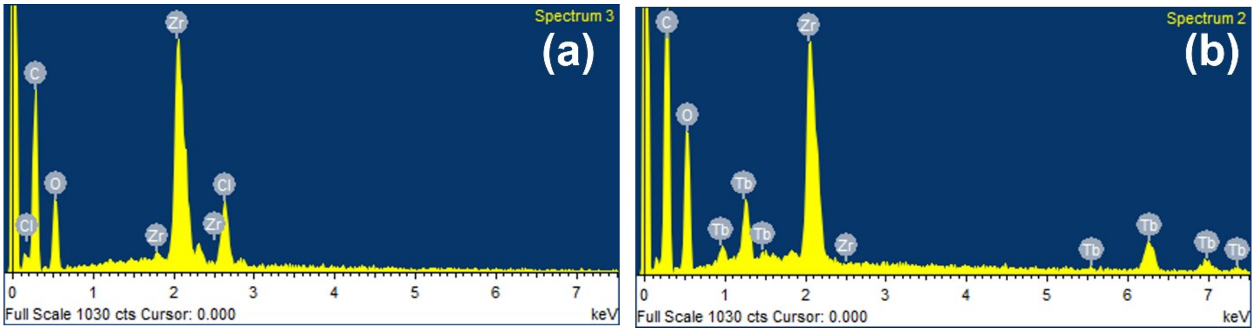

Figure S4. EDS spectra of (a) ZrBTB and (b) ZrBTB-bzpdc-Tb-120. Chlorine element is from the HCl-based washing step for removing coordinated benzoate during the synthesis of ZrBTB, and it can be completely removed after performing the installation of terbium.[1]

ICP-OES experiments were conducted to quantify the atomic ratio between terbium and zirconium in each material; see detailed protocols for preparing ICP-OES samples in our previous work.[1] The obtained results are listed in Table S1.

Table S1. ICP-OES results.

Material	Tb atoms per Zr_6 node
ZrBTB-bzpdc-Tb-60	1.0
ZrBTB-bzpdc-Tb-80	1.5
ZrBTB-bzpdc-Tb-100	2.1
ZrBTB-bzpdc-Tb-120	3.3
ZrBTB-Tb-120	4.4

^1H NMR spectrum of the H_2bzpdc ligand dissolved in dimethyl sulfoxide-d6 is shown in Figure S5(a), which reveals two sets of doublet peaks originating from eight hydrogen atoms on the two phenyl rings of the ligand. Each bzpdc-functionalized MOF material was thereafter digested in concentrated D_2SO_4 and thereafter diluted with dimethyl sulfoxide-d6 for collecting the ^1H NMR spectrum of the sample; see detailed protocols for preparing NMR samples in our previous studies.[1, 2] One set of strong peaks located at around 7.9 ppm can be observed in the NMR spectra of all ZrBTB-containing samples displayed in Figure S5(b-f), which correspond to fifteen hydrogen atoms on the four phenyl rings of H_3BTB.[1, 3, 4] According to the crystalline structure of ZrBTB, the ratio between the BTB linker and the hexa-zirconium node is 2. Thus, the integrated peak areas shown in Figure S5(b) indicate that there are on average 1.4 bzpdc ligands per BTB linker, and thus 2.8 bzpdc ligands coordinated on each hexa-zirconium node of the ZrBTB-bzpdc. Similar quantifications were then performed for all other materials containing bzpdc, and the loadings are listed in Table S2. In addition, NMR spectra of all terbium-containing materials showing the singlet peak originating from three hydrogen atoms of acetate are plotted in Figure S6. Number of acetate ions per node in each material was then quantified according to the obtained acetate-to-BTB ratio in the digested sample, as listed in Table S2. From both NMR and ICP-OES data, ratios between acetate and terbium were also calculated, as listed in Table S2.

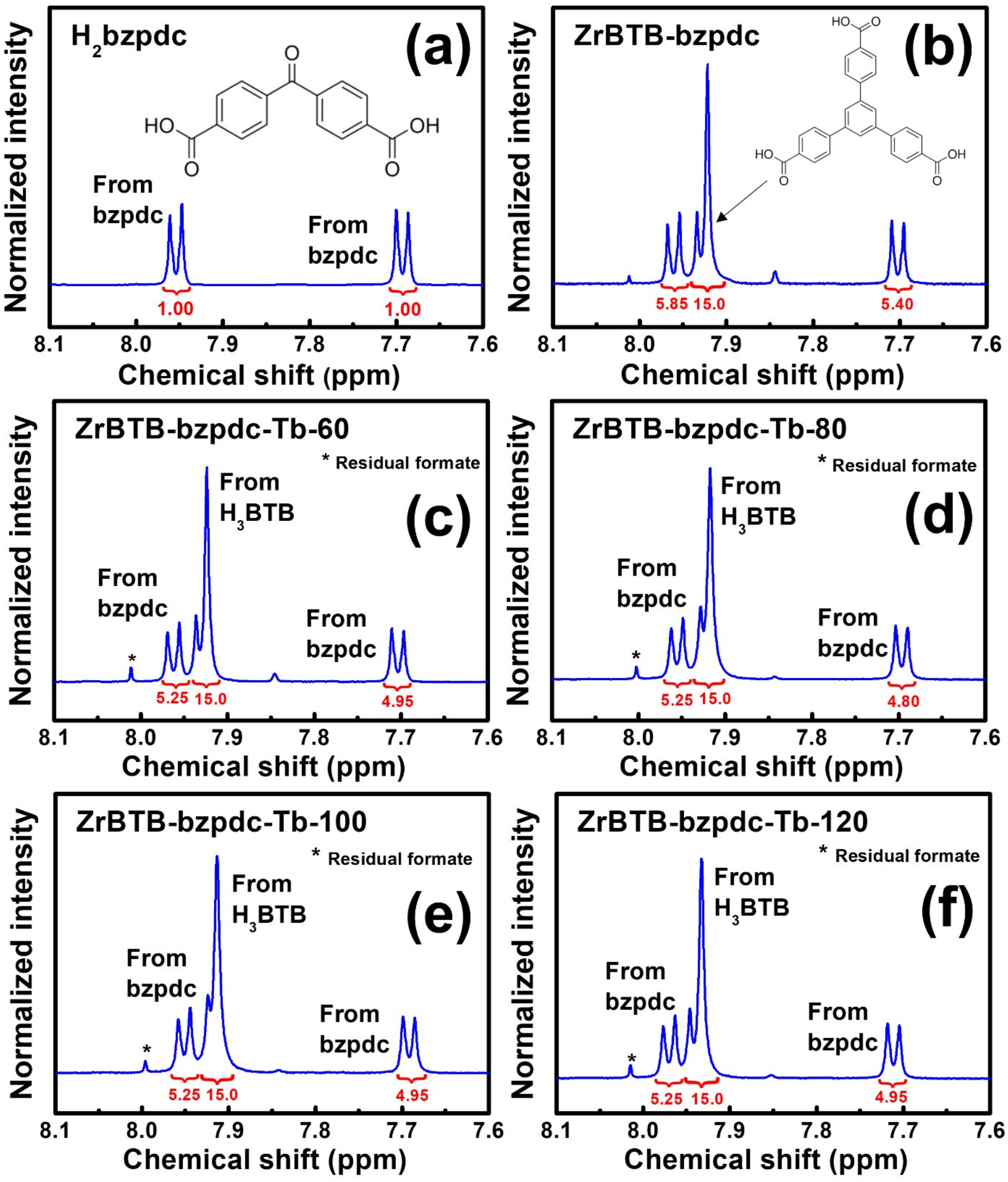

Figure S5. ^{1}H NMR spectra of (a) H_2bzpdc, (b) digested ZrBTB-bzpdc, (c) digested ZrBTB-bzpdc-Tb-60, (d) digested ZrBTB-bzpdc-Tb-80, (e) digested ZrBTB-bzpdc-Tb-100 and (f) digested ZrBTB-bzpdc-Tb-120, plotted in the region between 7.6 and 8.1 ppm.

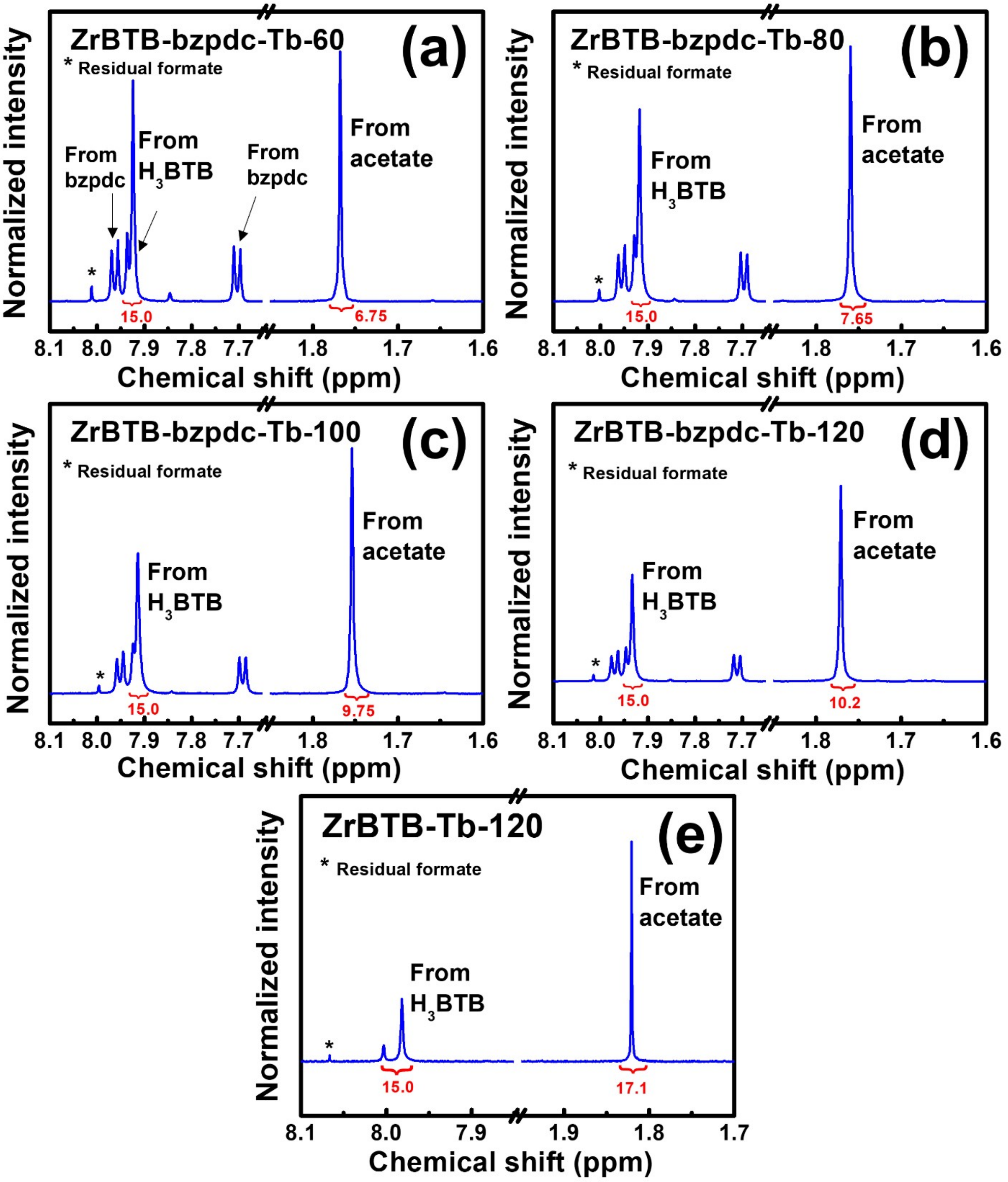

Figure S6. ^{1}H NMR spectra of digested (a) ZrBTB-bzpdc-Tb-60, (b) ZrBTB-bzpdc-Tb-80, (c) ZrBTB-bzpdc-Tb-100, (d) ZrBTB-bzpdc-Tb-120 and (e) ZrBTB-Tb-120, plotted in the regions covering both the peaks from H_3BTB and acetate.

Table S2. NMR results and ratios between acetate and terbium calculated from both NMR and ICP-OES data.

Material	bzpdc per Zr_6 node	Acetate per Zr_6 node	Acetate/Tb
ZrBTB-bzpdc	2.8	0	-
ZrBTB-bzpdc-Tb-60	2.5	4.5	4.5
ZrBTB-bzpdc-Tb-80	2.5	5.1	3.4
ZrBTB-bzpdc-Tb-100	2.5	6.5	3.1
ZrBTB-bzpdc-Tb-120	2.5	6.8	2.0
ZrBTB-Tb-120	0	11.4	2.6

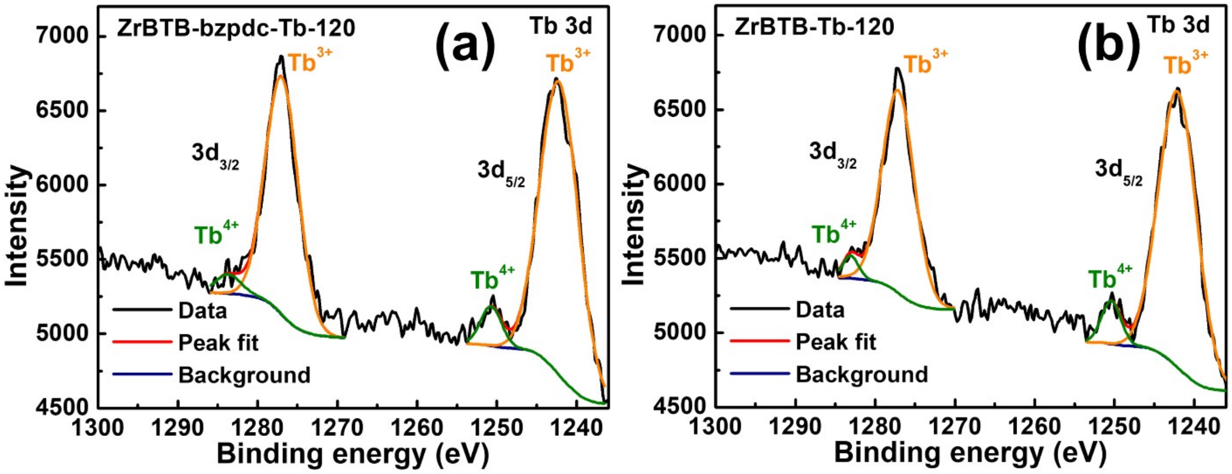

Figure S7. XPS spectra of (a) ZrBTB-bzpdc-Tb-120 and (b) ZrBTB-Tb-120, collected in the region of Tb 3d.

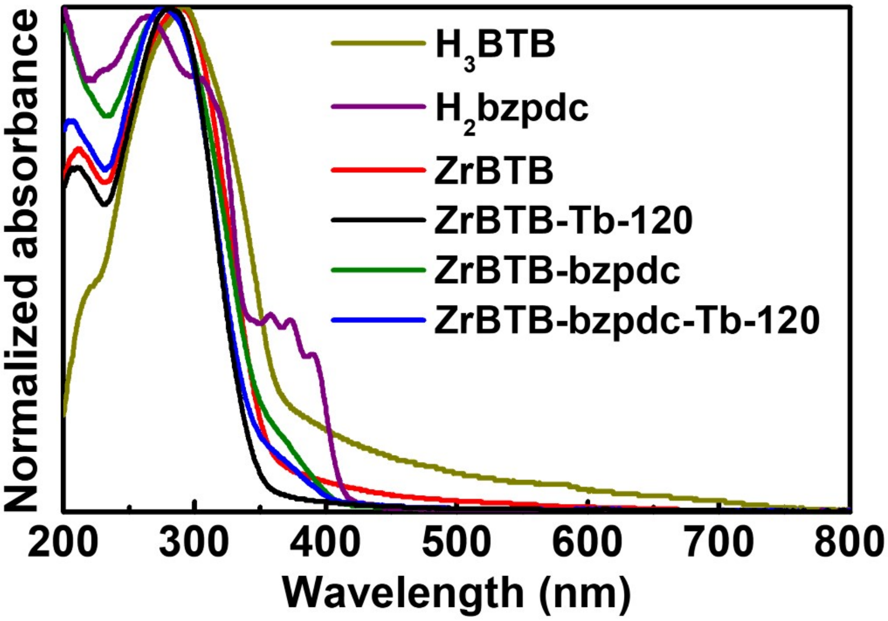

Figure S8. UV-vis spectra of ZrBTB, ZrBTB-bzpdc, ZrBTB-bzpdc-Tb-120 and ZrBTB-Tb-120. Spectra of H_3BTB and H_2bzpdc are also shown for comparison.

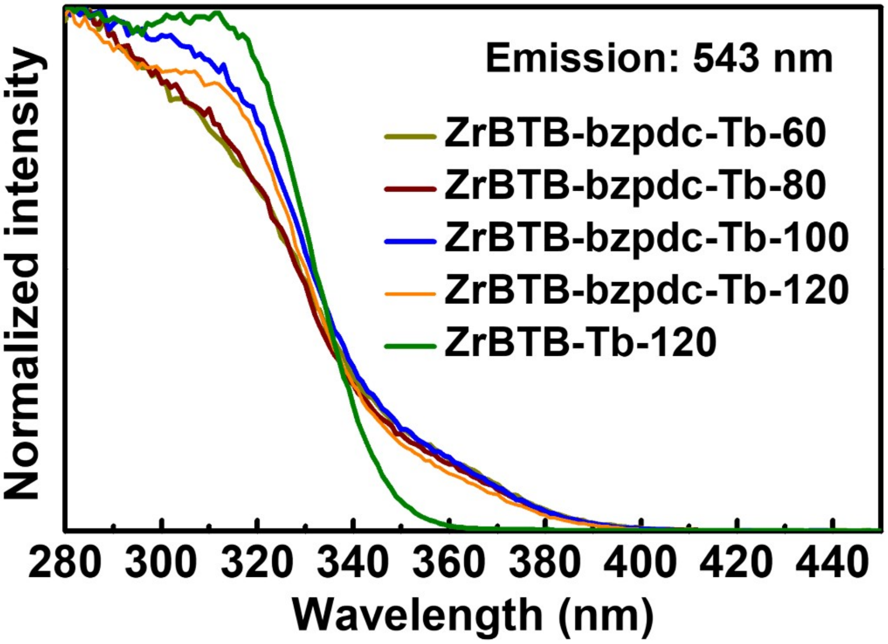

Figure S9. Excitation spectra of all terbium-functionalized 2D MOFs, collected by probing the emission of terbium at 543 nm.

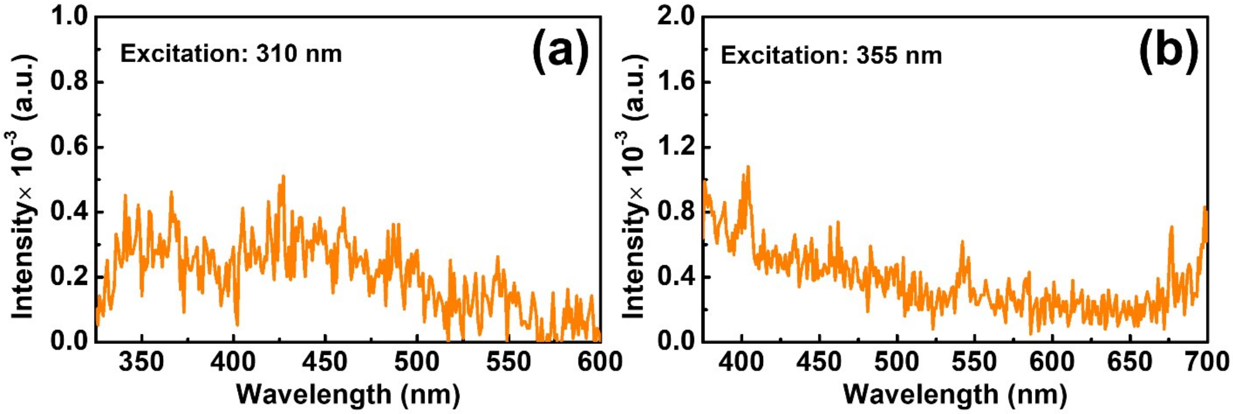

Figure S10. Emission spectra of the H_2bzpdc aqueous solution with a concentration of 0.2 mg/mL, collected under the excitation at (a) 310 nm and (b) 355 nm.

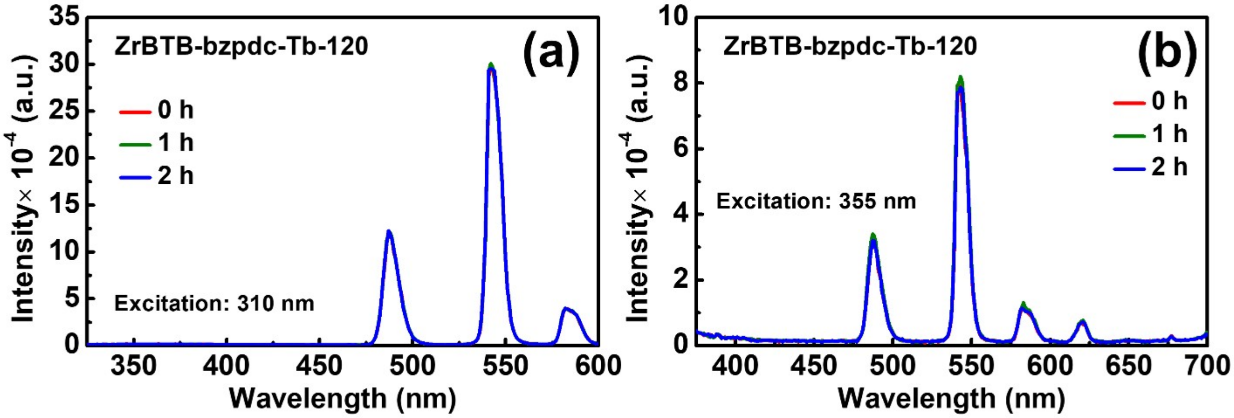

Figure S11. Emission spectra of the aqueous suspension of ZrBTB-bzpdc-Tb-120 with a concentration of 0.2 mg/mL, collected before and after keeping at room temperature for 1 h and 2 h. Spectra were collected under the excitation at (a) 310 nm and (b) 355 nm. The suspension was ultrasonicated before measuring each spectrum.

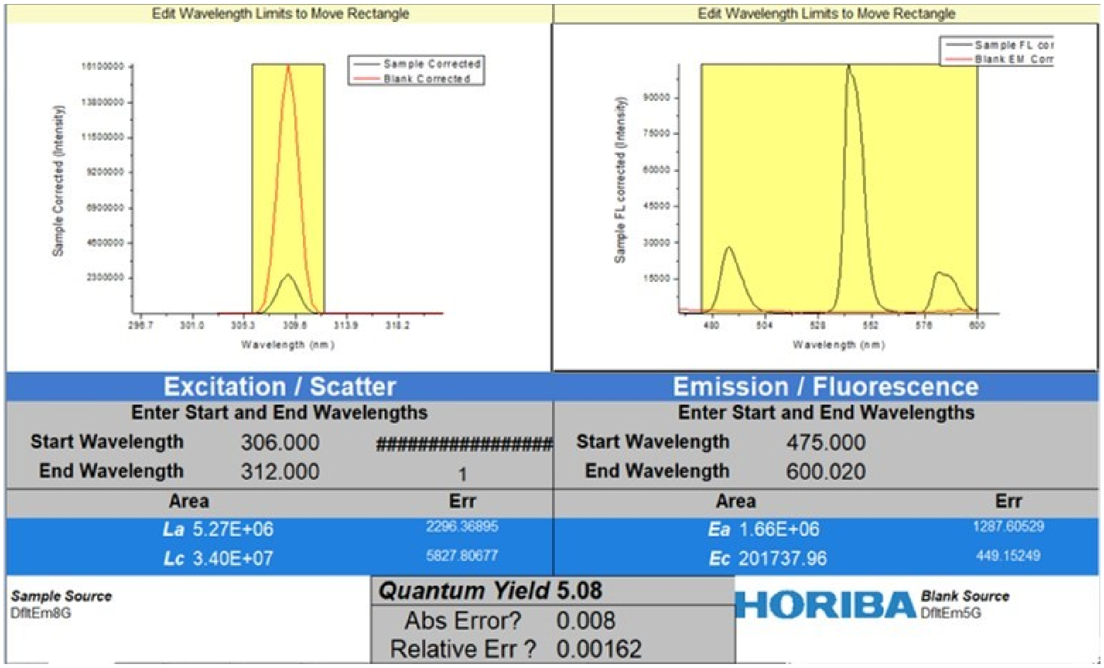

Excitation / Scatter

Enter Start and End Wavelengths

Start Wavelength 306.000 ##################

End Wavelength 312.000 1

Area	**Err**
La 5.27E+06	2296.36895
Lc 3.40E+07	5827.80677

Emission / Fluorescence

Enter Start and End Wavelengths

Start Wavelength 475.000

End Wavelength 600.020

Area	**Err**
Ea 1.66E+06	1287.60529
Ec 201737.96	449.15249

Sample Source
DfltEm8G

Quantum Yield **5.08**
Abs Error? 0.008
Relative Err ? 0.00162

Blank Source
DfltEm5G

Figure S12. Data of the PLQY measurement for ZrBTB-bzpdc-Tb-120 solid powder, under the excitation at 310 nm.

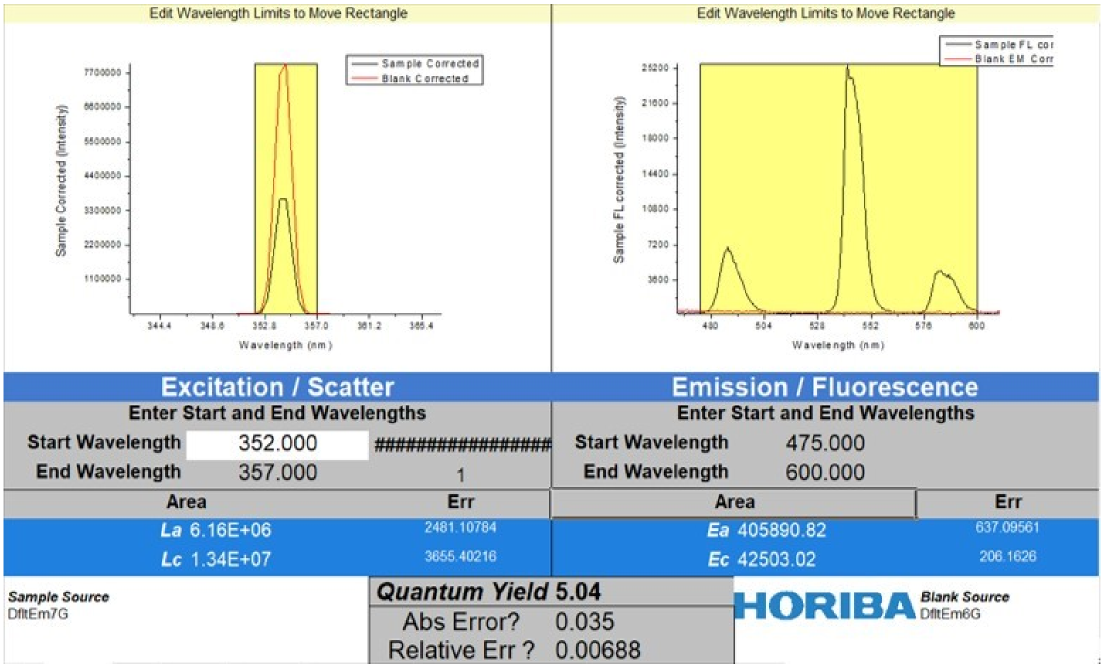

Excitation / Scatter

Enter Start and End Wavelengths

Start Wavelength 352.000 ##################

End Wavelength 357.000 1

Area	**Err**
La 6.16E+06	2481.10784
Lc 1.34E+07	3655.40216

Emission / Fluorescence

Enter Start and End Wavelengths

Start Wavelength 475.000

End Wavelength 600.000

Area	**Err**
Ea 405890.82	637.09561
Ec 42503.02	206.1628

Sample Source
DfltEm7G

Quantum Yield **5.04**
Abs Error? 0.035
Relative Err ? 0.00688

Blank Source
DfltEm6G

Figure S13. Data of the PLQY measurement for ZrBTB-bzpdc-Tb-120 solid powder, under the excitation at 355 nm.

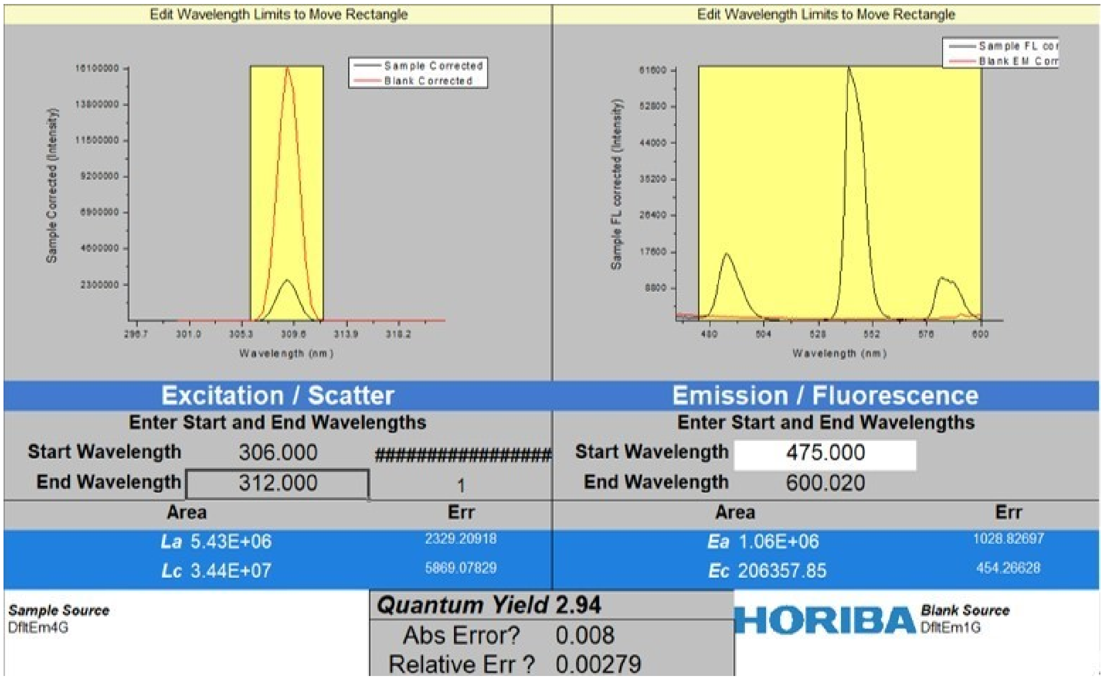

Excitation / Scatter			Emission / Fluorescence	
Enter Start and End Wavelengths			Enter Start and End Wavelengths	
Start Wavelength	306.000	##################	Start Wavelength	475.000
End Wavelength	312.000	1	End Wavelength	600.020

Area	Err	Area	Err
La 5.43E+06	2329.20918	*Ea* 1.06E+06	1028.82697
Lc 3.44E+07	5869.07829	*Ec* 206357.85	454.26628

Sample Source
DfltEm4G

Quantum Yield 2.94
Abs Error? 0.008
Relative Err ? 0.00279

Blank Source
DfltEm1G

Figure S14. Data of the PLQY measurement for ZrBTB-Tb-120 solid powder, under the excitation at 310 nm.

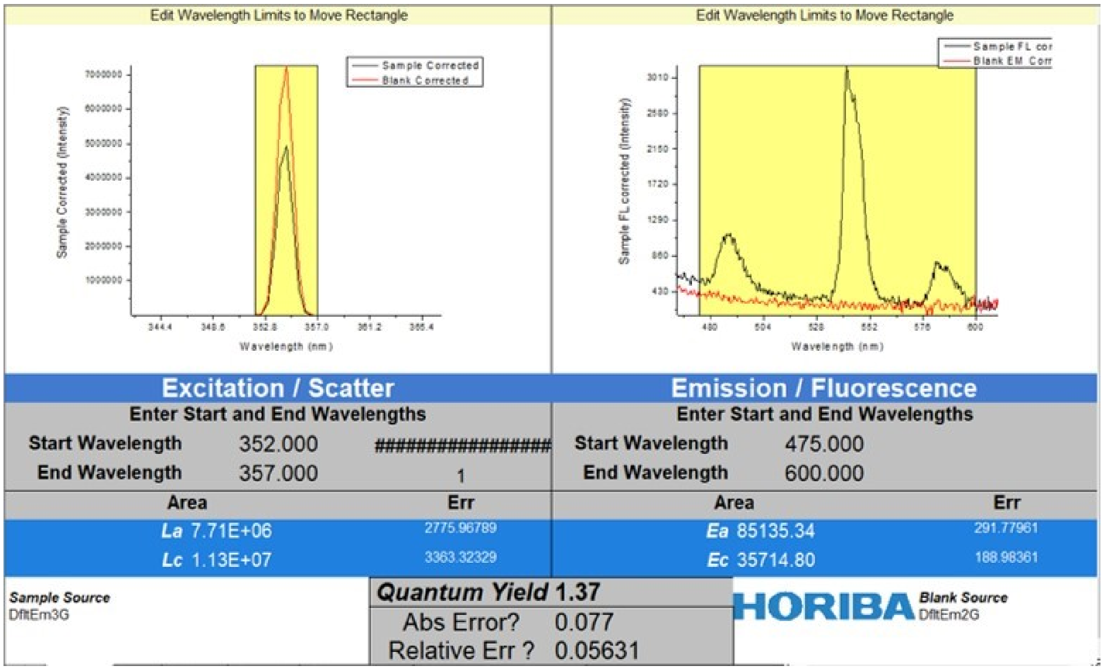

Excitation / Scatter			Emission / Fluorescence	
Enter Start and End Wavelengths			Enter Start and End Wavelengths	
Start Wavelength	352.000	##################	Start Wavelength	475.000
End Wavelength	357.000	1	End Wavelength	600.000

Area	Err	Area	Err
La 7.71E+06	2775.96789	*Ea* 85135.34	291.77961
Lc 1.13E+07	3363.32329	*Ec* 35714.80	188.98361

Sample Source
DfltEm3G

Quantum Yield 1.37
Abs Error? 0.077
Relative Err ? 0.05631

Blank Source
DfltEm2G

Figure S15. Data of the PLQY measurement for ZrBTB-Tb-120 solid powder, under the excitation at 355 nm.

Table S3. Performances of MOF-based PL sensors for Fe(III) ions in water reported in some published studies. The list is sorted based on K_{SV}.

Materials	K_{SV} (M^{-1})	LOD (μM)	Reference
Tb-based MOF (NIIC-1-Tb)	383000	0.00862	[5]
Eu-based MOF (NIIC-1-Eu)	28400	0.58	
Zr-based MOF-808-Tb	31200	N.A.	[6]
Eu-based MOF	31000	1.57	[7]
Tb-based MOF	28900	0.91	
Eu-based MOF	22300	1.12	[8]
Eu-based MOF (JXUST-9)	21340	0.94	[9]
ZrBTB-bzpdc-Tb-120	8970	2.8	This work
Tb-based MOF	8660	0.91	[10]
Tb-based MOF	5532	4	[11]
Eu-based MOF	4100	N.A.	[12]
Eu@Zr-based UiO-66	3780	12.8	[13]
Tb-based MOF	3530	2.22	[14]
Eu-based MOF	3660	2.09	
Tb-based MOF (Tb-DSOA)	3543	N.A.	[15]
Tb-based MOF (CTGU-1)	2400	0.1	[16]

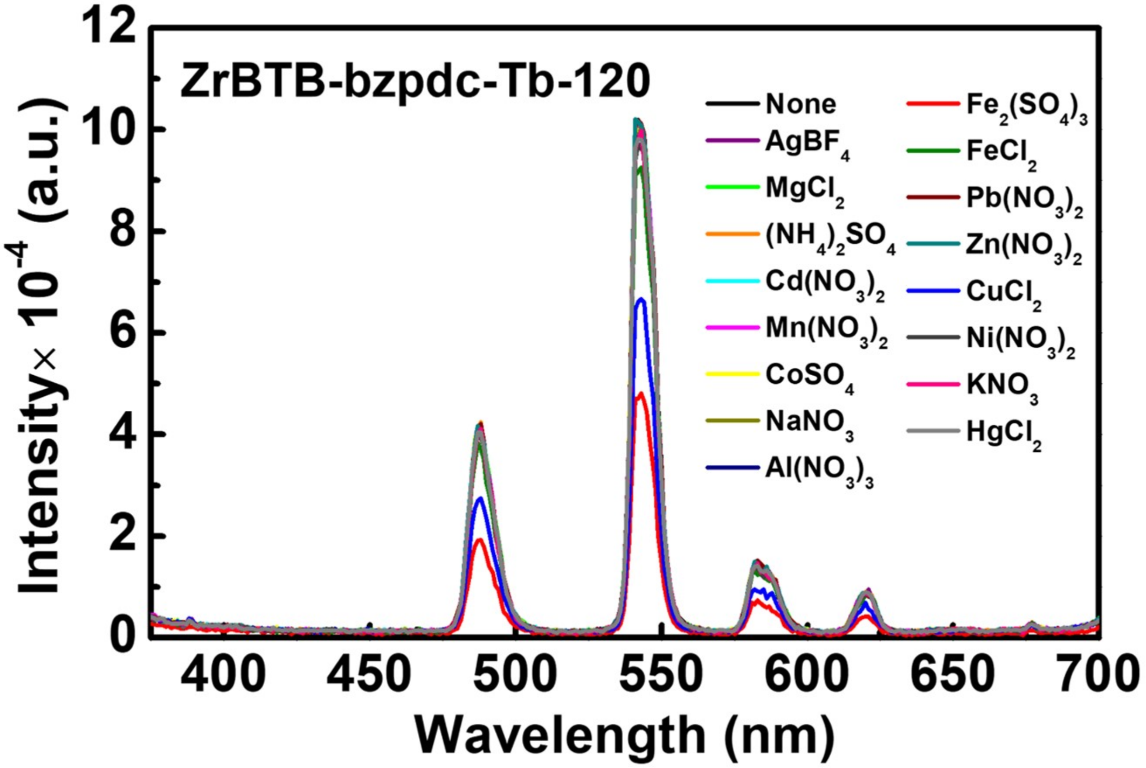

Figure S16. Emission spectra of ZrBTB-bzpdc-Tb-120 dispersed in water with a concentration of 0.2 mg/mL containing 100 μM of various added species, collected under the excitation at 355 nm.

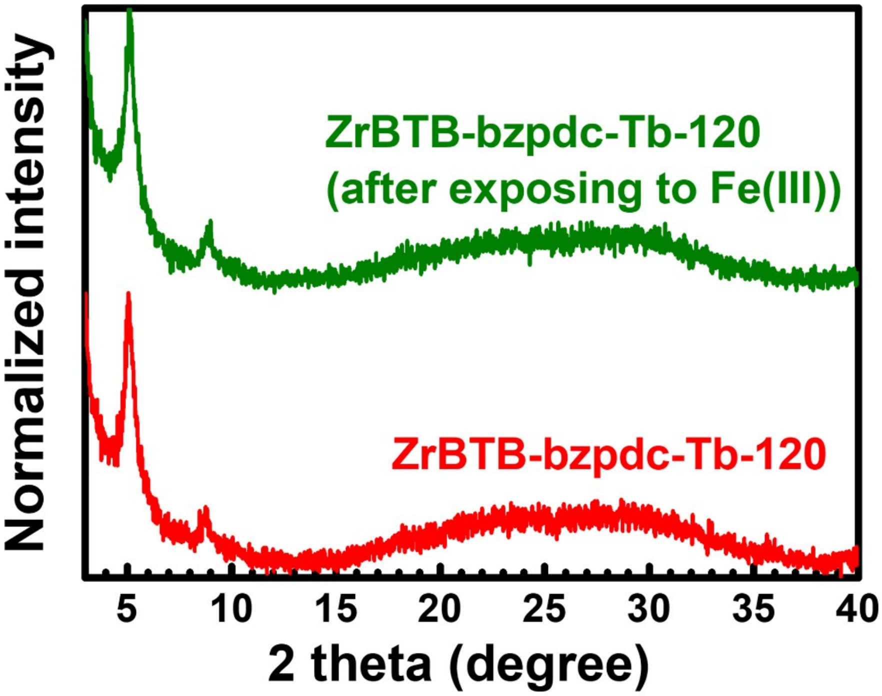

Figure S17. PXRD patterns of the fresh ZrBTB-bzpdc-Tb-120 and that after the exposure to the aqueous solution containing Fe(III) ions. Sample after exposure was prepared by dispersing 20 mg of ZrBTB-bzpdc-Tb-120 in 10 mL of an aqueous solution containing 50 μM of $Fe_2(SO_4)_3$ through ultrasonication, followed by keeping the obtained suspension at room temperature for 10 min, washing the resulting solid with 10 mL of water for three times, and subjecting to the solvent exchange with 10 mL of acetone for three times, sequentially, before activating the sample.

References:

1. Y.-L. Chen, C.-H. Shen, C.-W. Huang and C.-W. Kung, *Mol. Syst. Des. Eng.*, 2023, **8**, 330-340.
2. C.-H. Shen, Y.-N. Chang, Y.-L. Chen and C.-W. Kung, *ACS Materials Lett.*, 2023, **5**, 1938-1943.
3. M. Padmanaban, P. Müller, C. Lieder, K. Gedrich, R. Grünker, V. Bon, I. Senkovska, S. Baumgärtner, S. Opelt and S. Paasch, *Chem. Commun.*, 2011, **47**, 12089-12091.
4. Y.-B. Zhang, H. Furukawa, N. Ko, W. Nie, H. J. Park, S. Okajima, K. E. Cordova, H. Deng, J. Kim and O. M. Yaghi, *J. Am. Chem. Soc.*, 2015, **137**, 2641-2650.
5. X. Yu, A. A. Ryadun, D. I. Pavlov, T. Y. Guselnikova, A. S. Potapov and V. P. Fedin, *Angew. Chem. Int. Ed.*, 2023, **62**, e202306680.
6. J. Zhang, S. B. Peh, J. Wang, Y. Du, S. Xi, J. Dong, A. Karmakar, Y. Ying, Y. Wang and D. Zhao, *Chem. Commun.*, 2019, **55**, 4727-4730.
7. X. Mi, D. Sheng, Y. e. Yu, Y. Wang, L. Zhao, J. Lu, Y. Li, D. Li, J. Dou, J. Duan and S. Wang, *ACS Appl. Mater. Interfaces*, 2019, **11**, 7914-7926.
8. Y.-X. Sun, G. Guo, W.-M. Ding, W.-Y. Han, J. Li and Z.-P. Deng, *CrystEngComm*, 2022, **24**, 1358-1367.
9. Q.-Q. He, S.-L. Yao, T.-F. Zheng, H. Xu, S.-J. Liu, J.-L. Chen, N. Li and H.-R. Wen, *CrystEngComm*, 2022, **24**, 1041-1048.
10. X. Jing, J. Liu, M. Guo, G. Chen, G. Ren, J. Li, H. Qin, Z. Yao, Y. Wan, W. Song, H. Zeng, F. Yang, D. Zhao and K. Hu, *New J. Chem.*, 2023, **47**, 13619-13625.
11. K.-Y. Wu, L. Qin, C. Fan, S.-L. Cai, T.-T. Zhang, W.-H. Chen, X.-Y. Tang and J.-X. Chen, *Dalton Trans.*, 2019, **48**, 8911-8919.

12. M. Zheng, H. Tan, Z. Xie, L. Zhang, X. Jing and Z. Sun, *ACS Appl. Mater. Interfaces*, 2013, **5**, 1078-1083.

13. L. Li, S. Shen, W. Ai, S. Song, Y. Bai and H. Liu, *Sens. Actuators B Chem.*, 2018, **267**, 542-548.

14. Z.-D. Zhou, C.-Y. Wang, G.-S. Zhu, B. Du, B.-Y. Yu and C.-C. Wang, *J. Mol. Struct.*, 2022, **1251**, 132009.

15. X.-Y. Dong, R. Wang, J.-Z. Wang, S.-Q. Zang and T. C. W. Mak, *J. Mater. Chem. A*, 2015, **3**, 641-647.

16. M.-L. Han, G.-W. Xu, D.-S. Li, L. M. Azofra, J. Zhao, B. Chen and C. Sun, *ChemistrySelect*, 2016, **1**, 3555-3561.